frontiers | Frontiers in Earth Science

TYPE Original Research
PUBLISHED 18 September 2023
DOI 10.3389/feart.2023.1249787

Depositional environment variations and organic matter accumulation of the first member of the Qingshankou formation in the southern Songliao Basin, China

Yan Ma[1,2,3]* and Feng Jinlai[3]

[1]State Key Laboratory of Shale Oil and Gas Enrichment Mechanisms and Effective Development, Beijing, China, [2]SINOPEC Key Laboratory of Petroleum Accumulation Mechanisms, Wuxi, China, [3]Earth Science College, Northeast Petroleum University, Daqing, China

Check for updates

OPEN ACCESS

EDITED BY
Nagarajan Ramasamy,
Curtin University Sarawak, Malaysia

REVIEWED BY
Sharmila Bhattacharya,
Indian Institute of Science Education and Research Mohali, India
Quanyou Liu,
SINOPEC Petroleum Exploration and Production Research Institute, China
Numair Siddiqui,
University of Technology Petronas, Malaysia

*CORRESPONDENCE
Yan Ma,
185060862@qq.com

RECEIVED 29 June 2023
ACCEPTED 22 August 2023
PUBLISHED 18 September 2023

CITATION
Ma Y and Jinlai F (2023), Depositional environment variations and organic matter accumulation of the first member of the Qingshankou formation in the southern Songliao Basin, China.
Front. Earth Sci. 11:1249787.
doi: 10.3389/feart.2023.1249787

The organic-rich shale in the first member of the Qingshankou Formation, which is located in the southern Songliao Basin, is regarded as a high-quality source rock in East China. Geochemistry parameters were utilized to illustrate the formation and preservation conditions of the Qing1 Member in the Changling Sag, southern Songliao Basin. In the present study, from longitudinal continuity, the samples of organic geochemistry and elemental geochemistry were collected and systematically analyzed. This aims at determining the paleosalinity, paleoclimate, paleoredox conditions, and paleoproductivity and reconstructing its depositional paleoenvironment. According to total organic carbon (TOC) content, the Qing1 Member in the Changling Sag can be classified into two intervals, which are the lower part and the upper part, with high TOC content and low TOC content, respectively. It can be proved from the results of geochemical indicators that under warm and humid climatic conditions the relatively lower part was generated in the anoxic environment. Terrigenous input brought nutrients to the water body of the lake, made algae flourish, and had a relatively high paleoproductivity of the lake, which imposed a vigorous impact on the accumulation of organic matter. The upper part is mainly deposited under weakly oxidizing conditions, with gradually enhanced oxidation and reduced productivity. In contrast to the lower shale, the terrigenous inflow is relatively low. TOC content in the Qing1 Member has a positive relevance with the paleoredox conditions, as well as the paleosalinity conditions, indicating that good preservation is favorable for the accumulation of organic matter. A depositional model is proposed for the organic matter accumulation of this shale. The upper part was in a relatively hot and dry paleoclimate, with a low degree of organic matter enrichment, whereas the lower part had a warm and humid paleoclimate, with the input of terrestrial organic matter into the primary productivity of the lake basin and a high degree of organic matter enrichment.

KEYWORDS

organic matter, Songliao Basin, depositional environment, primary productivity, source rock

1 Introduction

Highly abundant in organic matter, shale is the source rock for the exploration of hydrocarbons. The accumulation of organic matter in rocks can be affected by various environmental factors such as main productivity, oxidation-reduction conditions of water column, and influx of terrestrial sources (Tribovillard et al., 1996; Li et al., 2017; Harris et al., 2018). Previous studies showed that developing source rocks with excellent quality mainly depends on the input and preservation of organic matter. Models describing the evolution of source rocks can be classified into different forms. 1) The "paleoproductivity model" refers to the high input of organic matter in a basin formed through paleoclimate, aquatic organisms in sedimentary water, and terrestrial organic matter supply. Oxygen is consumed by the water body to form a reductive environment, which is favorable for the preservation of organic matter in sediments (Mort et al., 2007; Li et al., 2017; Zhao et al., 2016; Yin et al., 2017; Tian et al., 2019). 2) The "preservation model" means that under a high deposition rate, paleo water depth, and poor hydrodynamic conditions, the absorbed organic matter is then effectively saved at the anoxic bottom of the aquatic environment in the process of enrichment of sedimentary organic matter (Carrol and Bohacs, 1999; Holfmann et al., 2000; Katz, 2005; Tyson, 2005). 3) The "paleoproductivity preservation interaction model" is the comprehensive result of high organic matter inputs and an anoxic environment (Huang et al., 2013; Jin et al., 2020). The key to establishing an accurate organic matter enrichment model is clarifying the paleosedimentary environment formed under the comprehensive control of various factors.

Although most oil shale exploration is concentrated in marine systems, in many countries, lacustrine mudstone plays a very essential role in shale oil exploration. In China, much of unconventional resource exploration, such as shale oil exploration, is concentrated in lacustrine formations. Different from the marine environment, the lake environment has the characteristics of a small scope, shallow water body, and many close material sources. The types of sediments are sensitive to changes in environmental factors such as climate. This reflects the lacustrine source rock has strong heterogeneity of oil and gas potential. Therefore, the reconstruction of the sedimentary environment is in need of urgent exploration to forecast the distribution of hydrocarbon and evaluate the potential of oil and gas. However, as mentioned above, the main factors commanding organic matter enrichment on the characters of source rocks will vary with changes in the deposition environment. Therefore, we should study the characteristics of the paleosedimentary environment of source rocks in different regions. The sedimentary environment will have a great impact on the geochemical characteristics of sediments. The reconstruction of the paleoenvironment of sedimentary rocks rich in organic matter can be studied by means of elemental geochemistry and organic geochemistry. Therefore, the content and ratio of elements in source rocks are usually adopted to analyze the conditions of the paleoenvironment (Algeo and Maynard, 2004; Tao et al., 2017). In addition, the characteristics of biomarker compounds are also effective indicators of ancient sedimentary environments, such as revealing the source of organic matter contained in the formation environment. It is very important to choose the parameters of inorganic geochemistry and organic geochemistry to mutually support and analyze the interpretation of ancient environments.

The Songliao Basin is the greatest continental petroliferous basin in China. In the late Cretaceous, the Qingshankou was the main stage for the expansion of the Songliao Basin. Among them, the Qing1 Member not only has been proven to be a series of excellent source rock development horizons with powerful hydrocarbon generation abilities but also is a main source rock and favorable reservoir rock, accompanied by extensive oil and gas display in the basin. However, previous research mainly focused on the northern Songliao Basin, including its source rock and reservoir characteristics, the composition of organic matter (OM) (Tu et al., 2012), and depositional filling developments (Zhang et al., 2018). There is little information about the southern section of the centrality depression in the Songliao Basin. Recently, with the deepening of shale oil exploration, the oil resource structure of the Songliao Basin has changed greatly. The shale oil exploration area of the Qing1 Member is showing good exploration potential. Therefore, it is indispensable to investigate the organic matter enrichment mechanism of the Qing1 Member to understand the enrichment of shale oil and gas. As an important source rock in the field, the formation environment of the Qingshankou Formation (k_2qn) has been controversial. Previous studies suggested that this series of origin rocks obtain main progress in the lacustrine sedimentary environment of fresh water to brackish water. Now more evidence demonstrates that the late Toulun period (the lower section of the Qingshankou formation) experienced large-scale transgression and hypoxia events (Hu et al., 2010), which provided important material basis and preservation conditions for the source rock formation. Under this background, the control and contribution of organic matter accumulation are still unclear. This does not help to explore the shale oil and gas resources in the research zones.

Previous researchers mostly used organic geochemical data to analyze the impact of the paleoenvironment on lacustrine source rock deposition and organic matter enrichment (Dong et al., 2015). However, this study conducted organic geochemical and elemental geochemical testing and analysis on shale system samples, providing a more comprehensive method. This method was first adopted at the Qing1 Member in the southern part of the Songliao Basin. To clarify the role of paleoenvironmental factors in organic matter enrichment, this study uses the indicators of element geochemistry and organic molecular geochemistry to reconstruct the sedimentary environment and analyzes the correlation between paleoenvironmental factors and organic carbon abundance. This research paper not only hopes to establish a sedimentary evolution model of organic matter accumulation but also provide a scientific basis for further investigation of shale oil in the research zone.

2 Geology setting

Situated in Northeast China, the Songliao Basin is a large north-northeast-trending Mesozoic–Cenozoic continental lacustrine basin. As one of the largest oil-bearing basins in China, it covers an area, length, and breadth that approximately reaches 2.6×10^5 km^2, 7.5×10^2 m, and $(3.3–3.7) \times 10^2$ m, respectively (Figure 1A). It derived from the basement in the Inner Mongolia

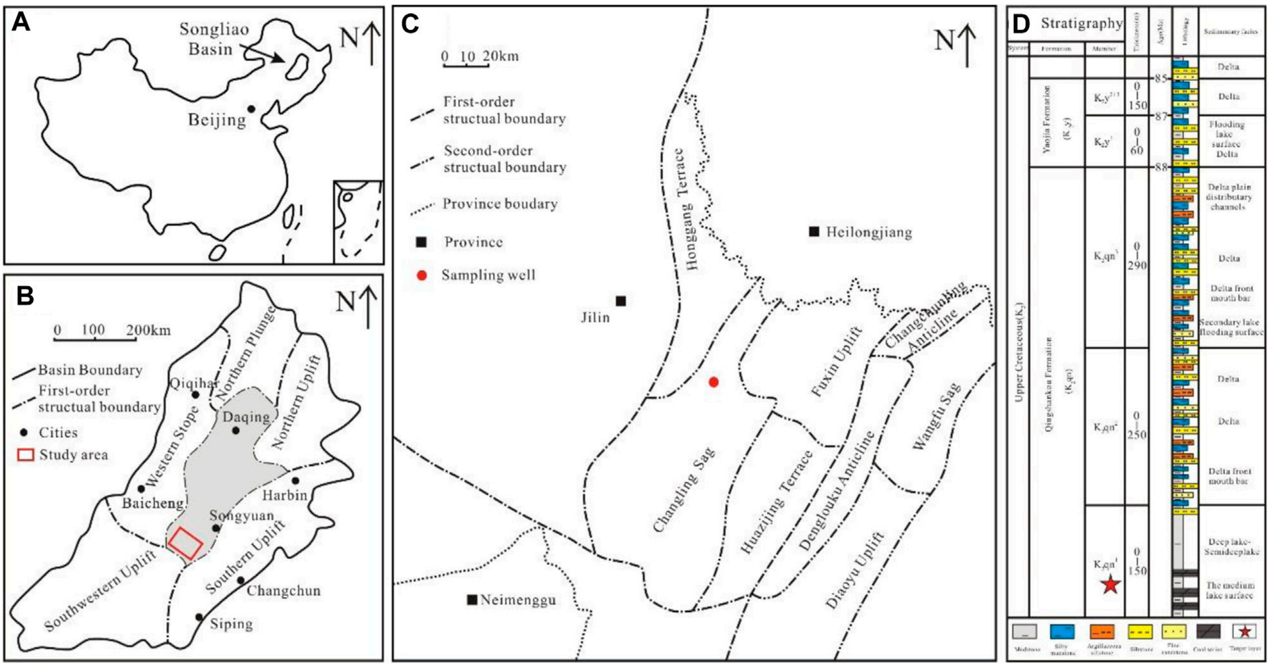

FIGURE 1
Map of six tectonic units in China **(A)**, the Songliao Basin **(B)**, exploration area **(C)**, and overall Lithology and stratigraphy of the Changling Depression **(D)** (the polished version from Liu et al., 2019).

and Jihei geosynclinal folds during the late Hercynian period (Wang et al., 2000a; Zhao et al., 2004; Hu et al., 2010). Since the Middle Jurassic, the Songliao Basin has experienced mantle upwelling due to plate tectonic interactions. This sustained until the Late Cretaceous (Zhang et al., 2016; Mizutani et al., 1989). Three major tectonic episodes occurred during the evolution of the basin: fault-related subsidence, thermal subsidence, and, finally, inversion (Liu et al., 2019; Wang et al., 2023). Specifically, during the Cretaceous rifting stage, the Pacific plate began to subduct below the Asian continent, forming a series of fault-bounded basins in northeastern China. In the middle Cretaceous, the lithosphere gradually cooled, resulting in extensive thermal subsidence of the basin with a corresponding increase in basin aerial extent (Wang et al., 2016). The central highlands eventually formed the central depression because of a strong thermal equilibrium adjustment in the underlying mantle. During the late Cretaceous, the deep structure of the basin continued to undergo equilibrium adjustment (Zhao et al., 2016). The lake basin gradually shrank, and the Songliao Basin was inverted by folding and uplift (Wei and Algeo, 2020). In accordance with the basement and tectonic evolution features, this basin consists of six first-order tectonic units, namely, the northern plunge, western slope, southwestern uplift, south-eastern uplift, northeastern uplift, and central depression (Figure 1B; Liu et al., 2019). Among them, the southern part of the center depression can be classified into four second-order structural components: 1) Honggang terrace; 2) Changling Sag; 3) Fuxin uplift belt; and 4) Huazijing terrace (Figure 1C).

Since the basin forming stage, the basin has mainly experienced three strong tectonic evolution stages, which control the deposition of strata above the basement. The basin can be roughly classified into three tectonic stratigraphic sequences separated by three regional unconformities, among which the Upper Cretaceous Qingshankou Formation corresponds to the post-rift stage (Wang et al., 2016). Among them, the Qingshankou Formation and Nenjiang Formation are the main oil and gas source beds. As a favorable source rock in the Songliao Basin, the Qingshankou Formation (K2qn) was sedimented in a medium-deep lake environment and was affected by global sea-level rise (Liu et al., 1993; Huang et al., 2013). The Qingshankou Formation is classified into three parts, namely, K2qn1, K2qn2, and K2q3, according to lithology (Figure 1D). Under the large-scale transgression, the first member of the Qingshankou Formation is extensively scattered and rich in organic matter, forming thick semi-deep lake lacustrine shale deposits and deep lake lacustrine shale deposits. Affected by basement subsidence (Zhong and Yang, 1978), the first member of the Qingshankou Formation has experienced several lake level rises during sedimentation, forming thick dark grey mudstone and shale deposits, with shale and fine-grained siltstone interbedding.

The Changling Depression is situated in the southern section of the central depression in the Songliao basin. As a vital hydrocarbon-generating depression in the basin, the sedimentary process of the Qingshankou formation has always been the focus of sedimentation and subsidence. The first member of the Qingshankou Formation was chosen as the goal horizon in the present study.

3 Materials and methods

A fresh 37 core samples was collected from the Qing1 Member (about 100 m) in the center of the Changling Sag. The lithology is

TABLE 1 Results of Rock-Eval pyrolysis parameters and TOC content of the Qing1 Member.

Part	Sample	Depth (m)	TOC (wt %)	S_1 (mg/g)	S_2 (mg/g)	HI (mg/g TOC)	T_{max} (°C)	Part	Sample	Depth (m)	TOC (wt %)	S_1 (mg/g)	S_2 (mg/g)	HI (mg/g TOC)	T_{max} (°C)
Upper part	T1-1	2340	1.09	0.47	6.72	273	434	Lower part	T1-20	2399.2	3.48	1.56	59.7	198	434
	T1-2	2342.1	1.11	0.34	2.35	223	439		T1-21	2401.9	1.8	1.29	24.10	246	442
	T1-3	2345	0.82	0.39	2.43	541	441		T1-22	2403.2	1.92	1.8	13.52	94	452
	T1-4	2348	0.81	0.06	1.98	469	441		T1-23	2404.5	2.46	2.31	19.28	81	437
	T1-5	2351	1.65	0.51	14.01	267	438		T1-24	2405	2.32	2.1	14.47	115	440
	T1-6	2353.9	0.87	0.11	0.84	402	433		T1-25	2407	3.69	21.22	49.5	132	435
	T1-7	2355	0.91	0.44	4.31	499	440		T1-26	2408.4	2.21	3.15	19.57	136	431
	T1-8	2358.03	0.84	0.58	6.57	537	437		T1-27	2410	2.93	5.21	31.1	134	429
	T1-9	2361	0.95	0.56	3.21	311	440		T1-28	2411.1	2.52	1.11	34.34	81	445
	T1-10	2363	0.95	0.95	2.35	352	431		T1-29	2411.86	1.5	2.36	15.64	52	447
	T1-11	2366	1.01	0.66	9.59	337	436		T1-30	2412.8	2.8	1.2	23.10	172	439
	T1-12	2370	1.11	0.7	5.21	308	444		T1-31	2416.7	2.12	19.11	25.89	176	445
	T1-13	2373	1.07	0.79	12.85	449	438		T1-32	2419.5	1.96	2.6	15.11	146	444
	T1-14	2375	0.95	0.76	6.58	364	435		T1-33	2421.5	2.01	1.23	14.23	220	433
	T1-15	2380	1.2	0.87	9.89	243	435		T1-34	2424.5	2.18	1.02	20.50	282	436
	T1-16	2382.2	1.3	0.64	11.07	432	442		T1-35	2426	2.22	2.01	28.77	308	441
	T1-17	2384.9	1.09	0.94	2.64	207	433		T1-36	2428.7	3.62	1.88	40.3	312	441
	T1-18	2386.1	0.81	1.09	8.65	205	433		T1-37	2434.2	3.31	15.26	27.49	154	434
	T1-19	2390	0.89	1.2	2.11	381	440								

Note: The S_1 peak value of Rock-Eval pyrolysis varies in a range of 1.02–21.22 mg HC/g rock in the lower part (4.8 mg on average) and 0.06–1.2 mg HC/g rock in the upper part (0.63 mg on average). The values of S_2 range from 13.52 to 59.7 mg HC/g rocks (26.4 mg on average) in the lower part to 0.84–14.01 mg HC/g rocks (5.96 mg on average) in the upper part.

mainly composed of gray-black shale, black mudstones, calcareous mudstone, and silty mudstones. The samples were selected from T_1 Well near the center of the Changling Sag, and can partly represent the characteristics of the Qing1 Member in this research zone. In total, 37 core samples (sample T_1-T_{19} represent the upper part and sample T_{20}-T_{37} represent the lower part) were utilized to determine the TOC content, elemental analysis and pyrolysis analysis, petrological characteristics analysis, and biomarker analysis.

3.1 Bulk organic geochemistry and organic petrography

Each rock sample was crushed and ground to less than 200 mesh (75–80um). Then, 200 mg of rock powder sample was put into a 5% dilute hydrochloric acid solution at 60°C, and washed to neutral with distilled water in the crucible. The washed sample was dried at 50°C for 24 h and placed in tin foil for packaging. We used the LECO CS-230 analyzer for TOC analysis. Approximately 60–100 mg crushed sample was heated in helium and kept at a constant temperature of 300°C for 3min. Then, we used the LECO CS-230 analyzer to analyze residual hydrocarbon S_1. First, we programmed the temperature at the rate of 50°C/min, and heated it at 300°C–600°C. We analyzed cracked hydrocarbon (S_2) and recorded the temperature (T_{max}) associated with the zenith on the peak of S_2. The analysis of organic lithofacies was carried out on the fluorescence microscope laborlux Photometer (MPV-3) with 12 pol micros. We used 50% at 23° ± 2°C × Objective at × 800 to collect the measured value with the total magnification.

3.2 Elemental analysis

X-ray fluorescence spectrometry was carried out to measure the concentration of the main elements. DI water was utilized to wash the samples many times, which were then dried. The samples were ground to 200 mesh (75–80 um) with agate mortar, heated to 1,000°C, and kept constant for 90 min. The weight reduction was recorded. The trace element test was to add the sample into the solvent of lithium metaborate and lithium tetraborate, mix evenly, dry at 105°C, cool the solution, fix the volume with HNO_3, HCl solution, and HF successively, and then complete the test with inductively coupled plasma mass spectrometer (ICP-MS). The environmental temperature of the laboratory and the relative humidity were, respectively, set at 20°C and 27%. Based on these conditions, the analytical precision of replicate analyses was less

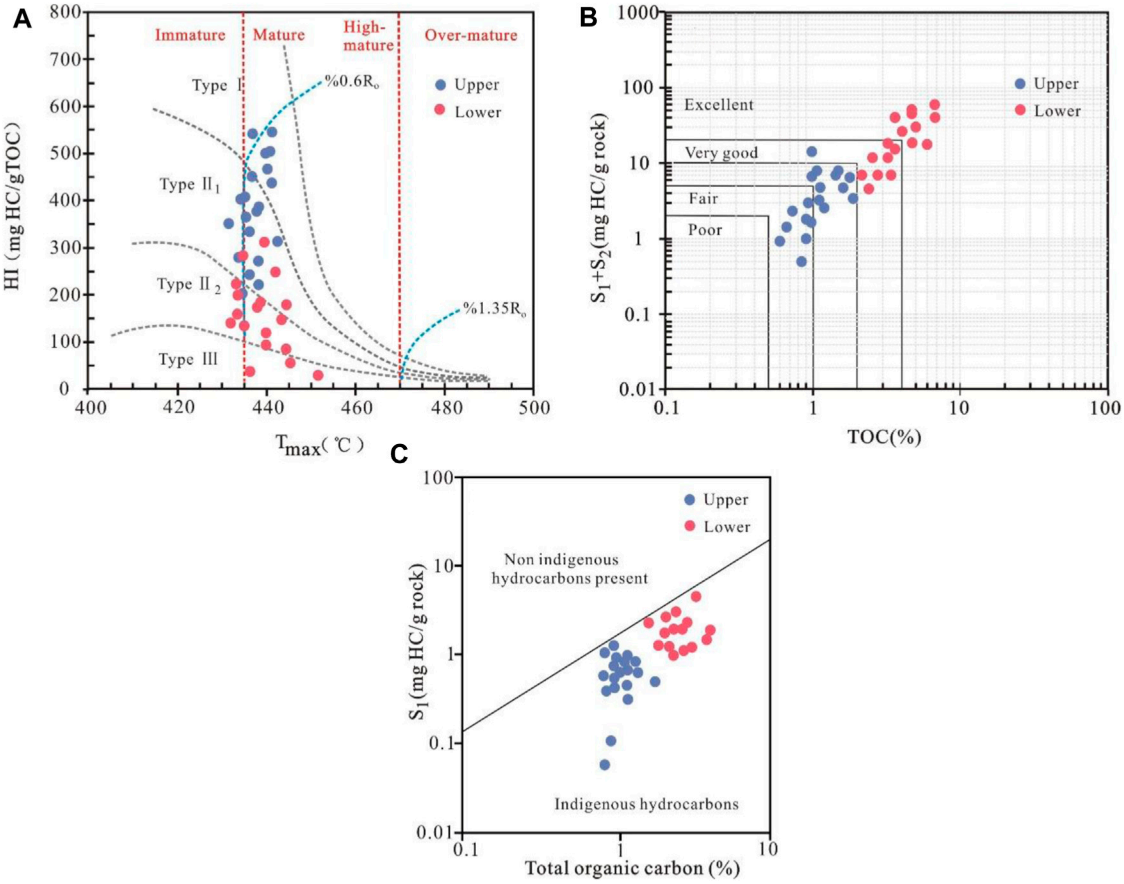

FIGURE 2
Source rock assessment graphic of the Qing1 Member: **(A)** HI values vs. Tmax values. **(B)** S_1+S_2 values vs. the content of TOC. **(C)** S_1 values vs. the content of TOC.

than 5%. The test approaches and process complied with the national standard GB/T 14506.30-2010.

3.3 Molecular compositions of saturated hydrocarbons

The rock sample was crushed and the soluble organic matter was extracted by a mixture of dichloromethane and methanol placed in a Soxhlet extractor for 72 h. Meanwhile, the extracts were concentrated, and asphaltenes were precipitated from a hexane–dichloromethane solution (80:1). The group components were separated by column chromatography. Saturated hydrocarbons and aromatics were eluted with C_6H_{14} and CH_2Cl_2 hexane solution (2:1), respectively. A gas chromatograph and Agilent 7890 GC-MS device were adopted to measure the concentration of the saturated hydrocarbons and aromatics. The corresponding parameters have been reported and were set as follows (Huang et al., 2013): 1) The fused quartz column in the analyzer was 30 m DB-5 MS (inner diameter 0.25 mm; film thickness 0.25 m); 2) the oven was heated from 70°C to 300°C at the rate of 3 °C/min while the constant temperature was maintained for 30 min. We set the scanning range of the mass charge ratio to 50–650 and the scanning time to 0.7 s. The peak area and relative concentration of each compound were measured by employing the Atlas 2000 (labsystems) software. The test approaches and process abided by the national standard GB/T18606-2017.

3.4 Data calculations

The index C-value and the chemical index of alteration (CIA) were applied as a proxy of weathering and paleoclimatic changes (Nesbitt and Young, 1982; Price and Velbel, 2003; Yan et al., 2010; Wang et al., 2020). C-value is expressed as C-value = Σ (Fe+Mn+Cr+Ni+V+Co)/Σ(Ca+Mg+Sr+Ba+K+Na) (Zhao et al., 2016). CIA is expressed as CIA=molar $[(Al_2O_3)/(Al_2O_3 + CaO^* + Na_2O + K_2O)] \times 100$, where CaO^* represents the CaO in silicate minerals. In our study, the CaO was corrected by phosphate (CaO^* = molar CaO-molar $P_2O_5 \times 10/3$). If the calculated CaO^* was less than the molar value of Na_2O, the CaO^* values were applied in the calculation. Otherwise, the molar values of Na_2O were used (McLennan, 1993).

Enrichment factors (EFs) of element concentration were usually utilized to assess the elemental enrichment or depletion (Tribovillard et al., 2006; Algeo and Li, 2020). This index is expressed as $X_{EF} = (X/Al)_{sample}/(X/Al)_{average\ shale}$, where X represents the target element. In this research work, the post-

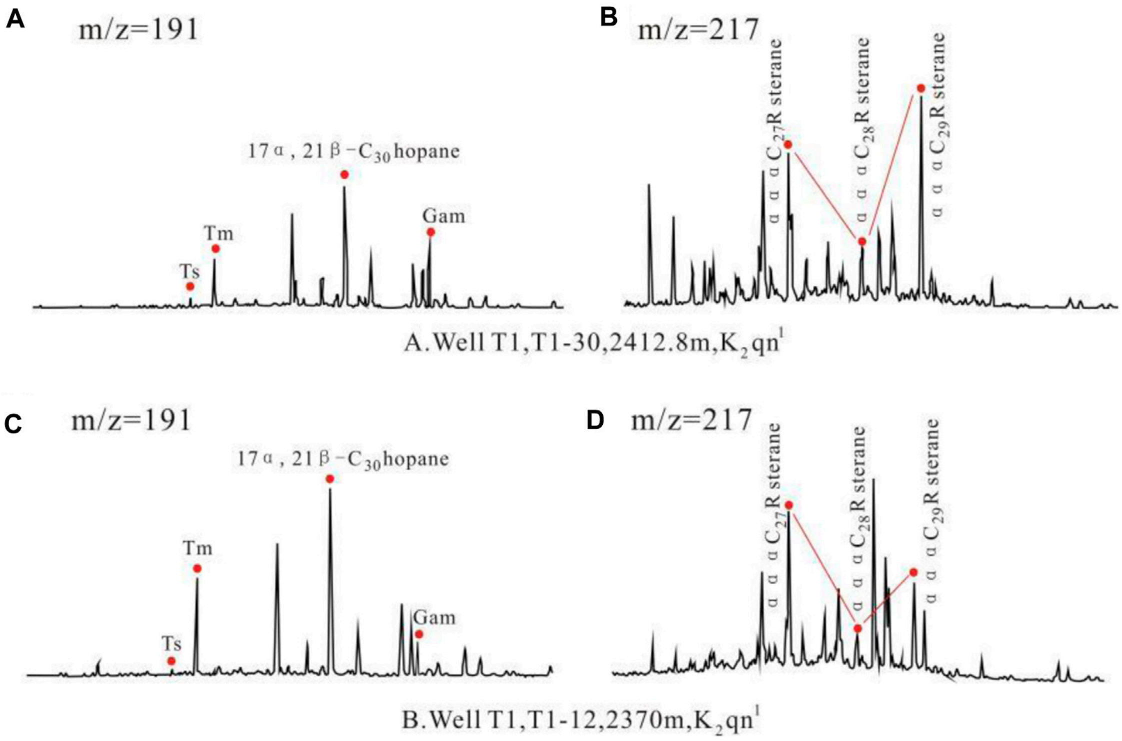

FIGURE 3
Chromatograms depicting the terpenoid distribution (m/z 191) and steroids (m/z 217) in the saturated hydrocarbon fractions in the Qing1 Member from the Changling Sag. Gam = gammacerane. Samples A **(A,B)** and B **(C,D)** were gathered from Well T1.

Archean Australian shale (PAAS) was selected as the reference standard. Meanwhile, XEF>1 and XEF<1 respectively reveal that the sample is enriched and depleted opposite to PAAS (Taylor and McLennan, 1985).

The Corg/P index is often used to indicate the redox conditions of water, calculated as the molar ratio of organic carbon to phosphorus. Corg/P=(organic carbon content/C element molar mass) (/P element content/P element molar mass) (Algeo and Ingall, 2007).

4 Results

4.1 Organic geochemical characteristics

Table 1 lists the TOC contents from the T1 well. The TOC contents of the shale increase from 0.81 wt% to 3.69 wt% (with a mean proportion of 1.74 wt%). The Qing1 Member is classified into two sections in line with its TOC content (Figure 2). One part is located at the lower part, and its TOC content is more than 2%. The TOC content in the lower part increased rapidly, up to 3.69 wt%. Subsequently, the TOC content increasingly declined and slightly fluctuated in the upper part. The other part is located in the upper part, and its TOC content is usually less than 2%. Meanwhile, the content of TOC in the upper part gradually descends (Figure 4).

Hydrogen index (HI = S_2/TOC × 100, mg HC/g TOC) values ranged from 52 to 312 mg HC/g TOC in the lower part (mean: 168 mg HC/g TOC) and 205–541 mg HC/g TOC (358 mg HC/g TOC on average) in the upper part (Table 1). The pyrolysis peak temperature values (Tmax, ∘C) varied from 429°C to 452°C (average: 439°C) in the lower part and 431°C to 444 °C (average: 437°C) in the upper part. The studied samples had indigenous hydrocarbons that were clearly observed from the cross-plot between free hydrocarbons (S1) vs. total organic carbon (TOC) in Figure 2C.

Figure 2 shows the relationship between HI and Tmax. It can be seen from the figure that both the mixture of type II_2 and type III kerogen in the lower part of the Qing1 Member is dominant and that type II_1 and type I kerogen in the upper part of the Qing1 Member is dominant.

Biomarkers are the molecular structures preserved after the death and burial of organisms with small changes. Biomarkers can be efficient in identifying both the origin of organic matter and changes in the deposition environment (Peters et al., 2005). In this research paper, the saturated hydrocarbons were analyzed, and the main compounds were identified according to their mass spectra. The main compounds showed peaks at m/z 191 and m/z 217.

C_{27}, C_{29}, and C_{28} steroids in the m/z 217 mass spectra of the shale in the Qing1 Member of the Changling Sag and constant steranes C_{27}–C_{28}–C_{29} in the upper part showed the distribution characteristics of C_{28}<C_{29}<C_{27} (Figure 3). The relative proportions of C_{27}, C_{28}, and C_{29} steranes varied in a range of 44.46%–72.23% (average: 61%), 15.81%–26.01% (average: 23.52%), and 6.13%–29.94% (average: 15.48%), respectively. The distribution characteristics of the lower part of regular steranes showed the

10.3389/feart.2023.1249787

TABLE 2 Content of main element data and trace element data of the T1 well in the Changling Sag of the Qing1 Member.

Part	Sample	Depth (m)	Major element (%)								Trace Element (ppm)					
			SiO_2	Al_2O_3	Fe_2O_3	CaO	K_2O	P_2O_5	TiO_2	Na_2O	Ba	Cu	V	Ni	Cr	Sr
Upper part	T1-1	2340	60.29	12.82	4.69	4.20	3.12	0.07	0.29	2.46	113.78	15.60	101.00	22.10	38.11	177.50
	T1-2	2342.1	43.03	13.17	7.35	7.42	1.60	0.28	0.31	2.30	213.33	37.50	98.70	27.80	64.09	348.00
	T1-3	2345	62.20	14.97	5.23	1.78	3.41	0.14	0.27	1.93	344.99	16.60	108.50	28.40	61.26	189.75
	T1-4	2348	59.28	13.57	4.52	1.72	3.40	0.51	0.30	2.30	371.35	18.10	97.50	26.80	53.57	189.39
	T1-5	2351	57.50	16.34	6.45	5.34	2.75	0.07	0.53	2.59	105.23	27.70	98.00	25.50	32.89	245.17
	T1-6	2353.9	56.23	16.10	4.32	4.28	3.00	0.18	0.62	2.05	259.81	21.10	83.40	27.00	56.35	174.08
	T1-7	2355	46.31	15.55	4.91	4.07	2.15	0.06	0.29	2.35	212.42	19.50	106.60	30.20	63.83	159.32
	T1-8	2358.03	56.12	14.85	7.83	7.52	3.64	0.13	0.51	1.67	212.98	28.00	112.70	33.10	65.14	259.84
	T1-9	2361	57.18	15.99	6.33	3.57	3.20	0.13	0.33	2.01	247.74	39.10	96.90	27.40	59.45	317.10
	T1-10	2363	58.63	15.37	5.67	2.18	3.50	0.08	0.28	2.03	271.67	32.90	92.00	20.80	51.11	358.61
	T1-11	2366	57.34	16.32	5.62	2.06	3.52	0.18	0.49	1.76	328.81	36.80	99.50	28.20	75.95	404.43
	T1-12	2370	49.44	10.02	4.52	5.23	2.52	0.06	0.17	2.04	273.66	39.60	108.70	29.70	33.86	451.44
	T1-13	2373	59.30	12.27	5.80	2.33	3.72	0.07	0.33	1.86	165.08	27.70	86.70	28.50	71.65	238.22
	T1-14	2375	56.89	12.98	4.58	0.89	3.58	0.07	0.43	1.10	108.08	19.30	116.40	27.30	106.79	156.72
	T1-15	2380	60.09	14.02	5.22	1.54	3.47	0.07	0.47	1.58	174.34	27.10	67.20	34.50	49.78	205.15
	T1-16	2382.2	56.63	16.46	5.63	1.32	3.13	0.08	0.52	1.67	215.01	33.10	165.40	26.40	131.27	260.17
	T1-17	2384.9	54.10	16.27	5.20	1.28	3.13	0.14	0.51	1.60	301.41	33.70	108.20	50.30	81.35	268.25
	T1-18	2386.1	55.18	14.67	5.26	3.38	3.29	0.07	0.55	1.67	128.60	12.50	70.00	28.30	51.47	116.00
	T1-19	2390	51.46	12.15	5.83	1.61	3.06	0.08	0.47	1.49	317.67	16.30	118.50	30.40	65.47	142.95
Lower Part	T1-20	2399.2	57.37	19.96	5.80	1.28	3.41	0.08	0.69	1.56	82.46	58.90	99.80	23.60	24.70	185.54
	T1-21	2401.9	58.52	12.46	5.18	1.11	3.62	0.25	0.51	1.46	150.98	32.90	113.00	23.00	49.78	283.84
	T1-22	2403.2	57.38	15.15	5.95	1.22	3.73	0.22	0.37	1.33	144.97	28.70	112.40	30.30	63.15	226.16
	T1-23	2404.5	55.41	15.87	6.39	1.12	3.69	0.17	0.48	2.52	88.20	28.30	76.60	27.20	30.17	176.31
	T1-24	2405	56.19	15.40	5.76	1.70	3.96	0.15	0.55	2.31	116.26	41.60	107.70	30.30	44.69	226.70
	T1-25	2407	59.47	21.38	4.04	3.23	3.84	0.21	0.71	2.46	145.77	90.80	102.60	24.90	36.00	325.06
	T1-26	2408.4	49.25	16.46	5.31	1.57	3.25	0.20	0.69	2.17	173.96	51.20	121.10	25.30	53.35	306.18

(Continued on following page)

TABLE 2 (*Continued*) Content of main element data and trace element data of the T1 well in the Changling Sag of the Qing1 Member.

Part	Sample	Depth (m)	Major element (%)								Trace Element (ppm)					
			SiO_2	Al_2O_3	Fe_2O_3	CaO	K_2O	P_2O_5	TiO_2	Na_2O	Ba	Cu	V	Ni	Cr	Sr
	T1-27	2410	57.27	19.94	5.60	1.48	4.28	0.19	0.62	2.45	194.99	66.40	118.30	26.10	23.71	413.37
	T1-28	2411.1	58.50	16.75	3.93	6.67	4.25	0.06	0.42	2.37	77.22	38.80	73.80	25.60	28.94	230.12
	T1-29	2411.86	53.34	16.79	4.76	2.99	3.65	0.53	0.49	2.26	180.42	29.90	105.20	25.90	68.18	224.25
	T1-30	2412.8	55.49	16.60	5.17	1.36	4.10	0.06	0.59	2.10	107.51	39.20	96.70	24.70	34.54	237.59
	T1-31	2416.7	57.80	13.63	4.42	3.28	4.35	0.12	0.54	2.42	149.42	34.20	100.40	29.20	47.14	251.03
	T1-32	2419.5	55.95	18.30	6.38	3.53	3.51	0.17	0.56	2.38	81.34	30.80	122.90	23.00	64.68	126.90
	T1-33	2421.5	55.56	16.73	5.39	0.85	3.85	0.15	0.56	2.44	76.36	27.80	87.70	21.20	43.85	123.71
	T1-34	2424.5	56.46	18.22	5.76	2.65	4.47	0.17	0.63	2.41	127.35	43.40	90.60	18.00	56.27	155.37
	T1-35	2426	55.17	18.17	6.33	1.49	3.17	0.15	0.56	2.90	109.53	42.30	101.10	23.30	49.08	184.01
	T1-36	2428.7	55.77	18.07	6.44	2.76	3.83	0.15	0.65	2.54	141.55	78.60	127.40	29.50	44.55	312.83
	T1-37	2434.2	54.75	17.88	6.49	6.69	4.10	0.18	0.57	2.19	113.49	88.30	108.00	25.50	28.95	354.08

order $C_{29} > C_{28} > C_{27}$ (Figure 3). The relative proportions of C_{27}, $C_{28,}$ and C_{29} steranes ranged from 14.4% to 27.76% (average: 19.03%), 13.21%–27.9% (average: 22.23%), and 48.23% to 68.9 (average: 58.75%), respectively. Gammacerane is a type of C_{30} triterpane. The G/C_{30}H (Gammacerane/C_{30} hopane) values of the origin rocks from the upper section and the lower section of Qing1 Member were in the range of 0.11–0.42 (average:0.26) and 0.22–0.65 (average:0.45), respectively.

4.2 Elemental geochemistry characteristics

It usually is a big error to judge the accumulation or depletion of elements according only to their relative content. Terrestrial clastic and biogenic components often disturb and reduce the concentration of hydrogen-derived elements. This stemmed from the fact that aluminum is derived from aluminosilicate in terrigenous clastic minerals, while siliciclastic aluminates have little mobility during diagenesis. Therefore, aluminum-normalized enrichment factors (EFs) of element concentration were usually utilized to assess the elemental enrichment or depletion (Tribovillard et al., 2006; Algeo and Li, 2020).

The concentrations of major elements and trace elements in Qing1 Member are listed in Table 2. SiO_2, Al_2O_3, $Fe_2O_{3,}$ and CaO are the four main elements in the samples, which follow a range from 43.03% to 62.20% (average: 55.85%), 10.02%–21.38% (average: 15.74%), 3.93%–7.83% (average: 5.51%), and 0.85%–7.52% (average: 2.88%), respectively. The samples are rich in SiO_2 relative to Al_2O_3 and CaO.

The concentration of trace elements including V, Ni, Cu, Cr, Sr, and Ba used in this study increased from 67.2 to 165.4 ppm (mean: 102.73 ppm), 18–50.3 ppm (average: 27.2 ppm), 12.5–90.8 ppm (average: 36.60 ppm), 23.71–131.27ppm (average:54.19ppm), 116–451.44 ppm (average: 243.38ppm), and 76.36–371.35 ppm (average: 179.13 ppm), respectively.

5 Discussion

5.1 Primary productivity

The source of organic matter in sediments and the primary productivity of lacustrine surface water can be expressed by biomarkers, in which the distribution of steroids can be effectively characterized (Volkman et al., 1998). The relative abundances of C_{27}-C_{29} regular steranes are good indicators for source organic matter input. C_{27} and C_{28} steranes are believed to be related to marine algal influence, while C_{29} steranes generally indicate a contribution from land plant organic matter (Yin et al., 2017; Wang et al., 2020). Among the steroids determined in shale samples gathered from the upper section of the Qing1 Member, the abundance of C_{29} regular sterane is higher than C_{27} regular sterane and C_{28} regular steranes (Figure 3), and the kerogen types were I and II_1. In samples gathered from the lower section of the formation, C_{27} regular steranes and C_{29} regular steranes both dominated (Figure 3), and the kerogen types were II_2 and III. These findings indicate that both of them are mixed-source inputs. In the lower part, the inflow of terrestrial higher plants is dominant, whereas the input of aquatic

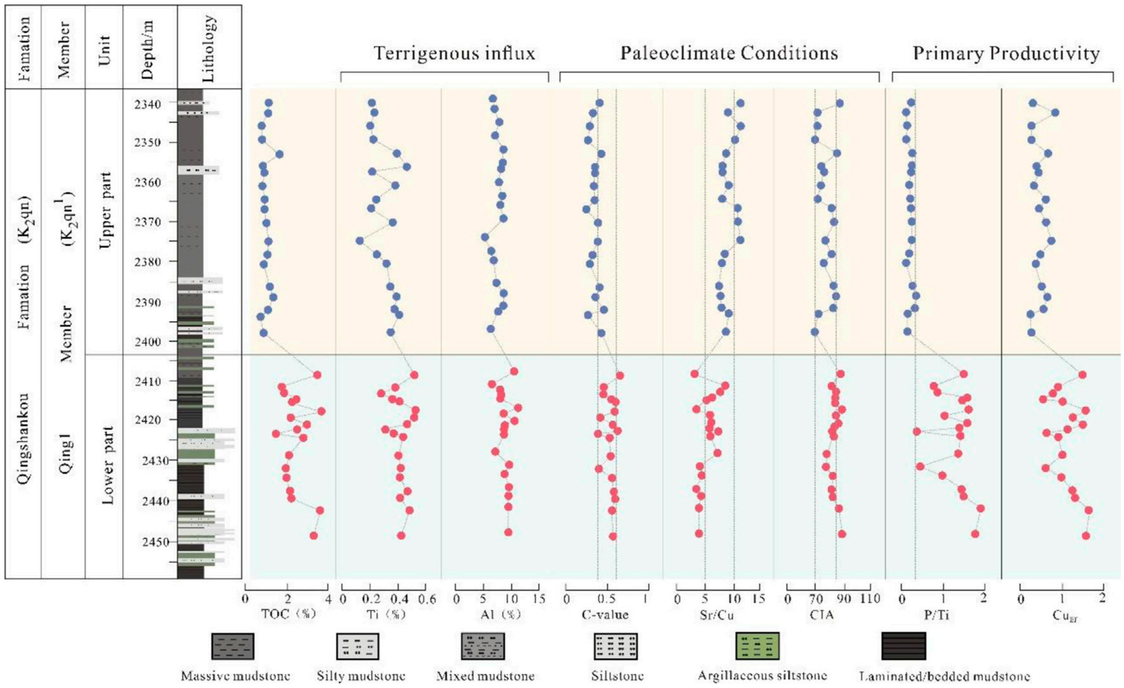

FIGURE 4
Variation curves of the terrigenous influx, paleoclimate, and primary productivity alternates of the Qing1 Member.

organisms and terrigenous influx both contributed in the upper section. In addition, high C_{19}/C_{23} tricyclic terpane ratios are usually indicative of terrigenous organic matter input (Dong et al., 2015). Samples from the upper part are characterized by relatively low C_{19}/C_{23} tricyclic terpane (average 0.59) (Table 2). In contrast, samples from the lower part are characterized by relatively high C_{19}/C_{23} tricyclic terpane (average 0.79). This may also indicate that the lower part source rock has more contribution from terrigenous organic matter compared to the upper part.

Productivity is an important factor affecting organic matter accumulation. Some trace elements (e.g., P, Ba, and Si) are employed to assess paleoproductivity (Tribovillard et al., 2006; Chen et al., 2020). P is indispensable for the growth of any organism. It is an essential nutrient for the high primary productivity of lake ecosystems (Schmitz et al., 1997; Schoepfer et al., 2015), and total phosphorus concentration is generally deemed as a salt compound for estimating primary paleoproductivity (Algeo and Ingall, 2007). P exhibits aggressive geochemical action in aquatic environments because it is often integrated into sediments in the form of organic matter or ferric hydroxide (Steiner et al., 2001). The ratio of P/Ti in the lower part of the investigation area is between 0.36 and 1.88 (average, 1.26), and that in the upper part is between 0.11 and 0.35 (average, 0.21). However, when compared with the P/Ti ratio of chert in the moderate-productivity Ubara profile (average, 0.34) (Liu et al., 2015), the values obtained in this study reveal that the paleoproductivity in the upper Qing1 Member in the Changling Sag shows a low level, while the lower part is relatively high (Figure 4).

However, the research shows that under anoxic conditions and the influence of redox conditions, elements such as P and Ba become more soluble (Yin et al., 2017). This may lead to the failure of their discriminant indexes. The concentration of Cu element is seen as a useful indicator to assess main productivity, which is due to the complexation reaction with organic matters, as well as the adsorption of iron manganese oxides or hydroxides with biological accumulation, leading to the Cu accumulation in the bottom sediments (Naimo et al., 2005). With the continuous enrichment of organic matter, Cu combines with organic matter and then precipitates. In a reducing environment, Cu is converted into Cu^{2+} or can combine with hydrosulfide to form CuS or CuS_2 (Pinedo et al., 2015). The Cu_{EF} value in the lower part of the Qing1 member varies from 1.12 to 3.25 (average: 2.22), and the Cu_{EF} value in the upper part varies from 0.48 to 1.68 (average: 0.94), suggesting that the paleoproductivity in the deposition of the lower part is higher than that of the upper part (Figure 4).

In Figure 10, there is a positive relevance between the abovementioned indicators and the content of TOC, revealing that paleoproductivity played an important role in organic matter accumulation (Figures 10A, B). In addition, based on the comprehensive analysis of paleoclimate and terrestrial input indicators examined in the following section, during the lower part sedimentation period, paleoproductivity was affected by the terrestrial influx. The warm and humid climate caused terrestrial input to bring nutrients to the lake basin water, and algae proliferated in large quantities, promoting paleoproductivity in the lake basin.

5.2 Paleoclimate conditions

The input of terrestrial organic matter and the primary productivity in aquatic environments are greatly affected by

TABLE 3 Geochemical indexes from T1 well of the Qing1 Member in the Changling Sag.

Part	Sample	Depth (m)	P/Ti	Cu_{EF}	C-value	Sr/Cu	CIA	Sr/Ba	G/C_{30}H	V/Cr	V/(V+Ni)	C_{org}/P	C19/C23 tricyclic terpane	Pr/Ph
Upper part	T1-1	2340	0.23	0.59	0.40	11.38	88.21	1.56	0.28	2.65	0.82	84.16	0.92	0.87
	T1-2	2342.1	0.12	1.68	0.32	9.28	72.01	1.63	0.37	1.54	0.79	89.23	0.45	0.66
	T1-3	2345	0.13	0.55	0.28	11.43	71.89	0.55	0.23	1.77	0.79	58.63	0.45	0.59
	T1-4	2348	0.12	0.56	0.26	10.46	70.12	0.51	0.16	1.82	0.79	98.50	0.63	0.62
	T1-5	2351	0.26	1.34	0.42	8.85	86.15	2.33	0.42	2.98	0.78	101.28	0.46	0.76
	T1-6	2353.9	0.25	0.77	0.35	8.25	75.01	0.67	0.16	1.48	0.75	69.46	0.58	0.82
	T1-7	2355	0.24	0.89	0.35	8.17	76.59	0.75	0.31	1.67	0.77	87.26	0.45	0.67
	T1-8	2358.03	0.19	0.65	0.33	9.28	74.56	1.22	0.19	1.73	0.76	66.23	0.78	0.58
	T1-9	2361	0.21	1.21	0.34	8.11	72.16	1.28	0.21	1.63	0.77	79.24	0.43	0.63
	T1-10	2363	0.23	0.88	0.24	10.90	82.15	1.32	0.15	1.80	0.80	52.34	0.43	0.85
	T1-11	2366	0.25	1.23	0.38	10.99	83.96	1.23	0.29	1.31	0.77	83.49	0.89	0.87
	T1-12	2370	0.25	1.48	0.38	11.40	77.65	1.65	0.33	3.21	0.78	110.25	0.66	0.9
	T1-13	2373	0.19	0.95	0.32	8.60	82.10	1.44	0.31	1.21	0.76	85.21	0.71	0.8
	T1-14	2375	0.11	0.75	0.29	8.12	76.77	1.45	0.12	1.09	0.81	48.71	0.45	0.73
	T1-15	2380	0.27	1.02	0.40	7.57	83.69	1.18	0.35	1.35	0.67	105.63	0.34	0.72
	T1-16	2382.2	0.35	1.29	0.35	7.86	85.49	1.21	0.39	1.26	0.89	111.23	0.67	0.68
	T1-17	2384.9	0.32	1.11	0.45	7.96	83.46	0.89	0.22	1.33	0.68	88.26	0.56	0.88
	T1-18	2386.1	0.16	0.48	0.26	9.28	72.36	0.90	0.25	1.36	0.71	52.36	0.67	0.75
	T1-19	2390	0.15	0.54	0.42	8.77	70.26	0.45	0.11	1.81	0.79	82.46	0.78	0.76
Lower Part	T1-20	2399.2	1.47	2.98	0.64	3.15	88.32	2.25	0.62	4.04	0.84	128.74	0.72	0.91
	T1-21	2401.9	0.78	1.78	0.45	8.63	82.76	1.88	0.26	2.27	0.88	102.39	0.69	0.88
	T1-22	2403.2	0.85	1.56	0.45	7.88	85.12	1.56	0.22	2.82	0.83	148.20	0.68	0.93
	T1-23	2404.5	1.54	1.12	0.55	6.23	85.26	2.00	0.54	3.12	0.77	146.85	0.89	1.11
	T1-24	2405	1.46	2.01	0.59	5.45	84.98	1.95	0.46	3.12	0.83	98.26	0.92	1.21
	T1-25	2407	1.59	3.10	0.58	3.58	89.38	2.23	0.62	3.09	0.84	156.48	0.77	1.19
	T1-26	2408.4	1.02	2.49	0.41	5.98	85.62	1.76	0.42	2.27	0.87	88.15	0.67	0.89
	T1-27	2410	1.56	2.99	0.57	6.23	86.59	2.12	0.48	4.99	0.87	144.57	0.45	0.91
	T1-28	2411.1	1.38	2.23	0.61	5.93	84.12	2.98	0.35	2.55	0.79	134.65	0.90	0.94
	T1-29	2411.86	0.36	1.25	0.38	7.50	82.16	1.24	0.30	3.24	0.86	98.79	1.08	1.04
	T1-30	2412.8	1.39	1.82	0.52	6.06	84.25	2.21	0.59	2.92	0.85	141.29	0.88	1.13
	T1-31	2416.7	1.35	2.01	0.53	7.34	78.59	1.68	0.45	2.91	0.83	139.80	1.01	0.94
	T1-32	2419.5	0.45	1.22	0.39	4.12	78.16	1.56	0.34	3.06	0.88	112.30	1.11	1.02
	T1-33	2421.5	0.97	1.96	0.55	4.45	83.26	1.62	0.38	3.03	0.85	121.20	0.67	1.13
	T1-34	2424.5	1.43	2.51	0.57	3.58	82.36	1.22	0.39	3.21	0.87	141.77	0.76	1.2
	T1-35	2426	1.48	2.63	0.58	4.35	83.26	1.68	0.38	3.07	0.83	132.59	0.88	0.94
	T1-36	2428.7	1.88	3.25	0.55	3.98	87.65	2.21	0.65	3.09	0.86	153.21	0.63	1.11
	T1-37	2434.2	1.75	3.12	0.56	4.01	89.63	3.12	0.61	3.03	0.85	148.55	0.56	0.96

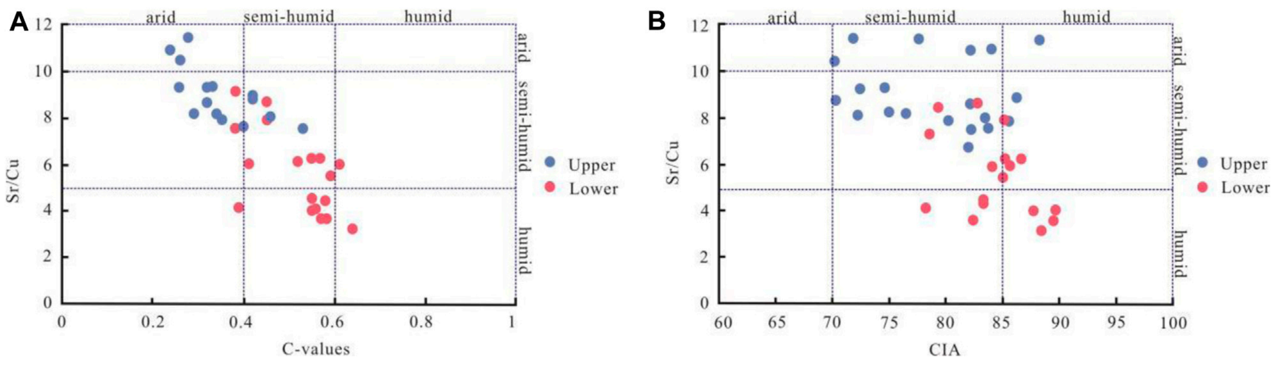

FIGURE 5
Crossplots of the paleoclimate proxies of the Qing1 Member. **(A)** C values vs. Sr/Cu ratios, cutoff values of 0.4–0.6 for C values and 5–10 for Sr/Cu are demonstrated as divisions for paleoclimate proxies; **(B)** CIA ratios versus Sr/Cu ratios, cutoff values of 70–85 for CIA and 5–10 for Sr/Cu are presented as divisions for paleoclimate proxies.

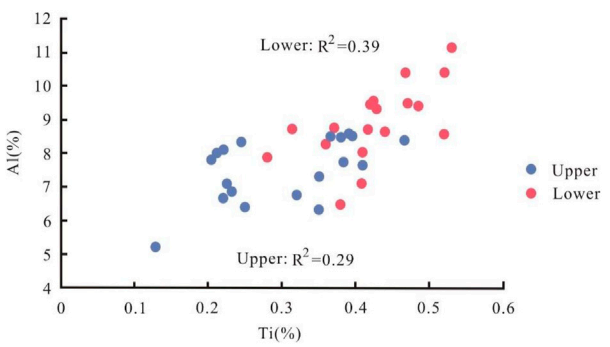

FIGURE 6
Strong positive relevance between Ti (%) and Al (%).

environmental temperature and humidity, which are controlled by climatic conditions (Tao et al., 2017). Generally speaking, a warm and humid climate has two sides. On the one hand, it can increase the direct runoff of the surface and improve main productivity. On the other hand, water stratification and main productivity will be promoted and inhibited, respectively (Chen et al., 2020).

The distribution and proportion of some trace elements in the sediments reflect the paleoclimatic conditions. It is commonly accepted that Fe, Mn, V, Cr, Ni, and Co are comparatively accumulated in moist environments, while Ca, Mg, K, Na, Sr, and Ba are accumulated in dry environments (Yin et al., 2017). Additionally, the C value has been well-used in the analysis of the Jurassic mudstone paleoclimate in the northern Qaidam Basin. Usually, the C value of less than 0.2, 0.2–0.4, 0.4–0.6, 0.6–0.8, and more than 0.80 indicates arid, semiarid, semiarid to semi-moist, semi-moist, and humid climatic conditions, respectively. As observed in Table 3, the C values of the upper part were 0.24–0.45 (mean 0.34), which reflects the average semiarid climate. The lower part had C values of 0.38–0.64 (mean 0.52), indicating a semiarid to semi-humid climate than the upper part.

The element Sr possesses a small ionic radius but high solubility and is easy to transfer in diagenesis. Therefore, the mobility of Sr

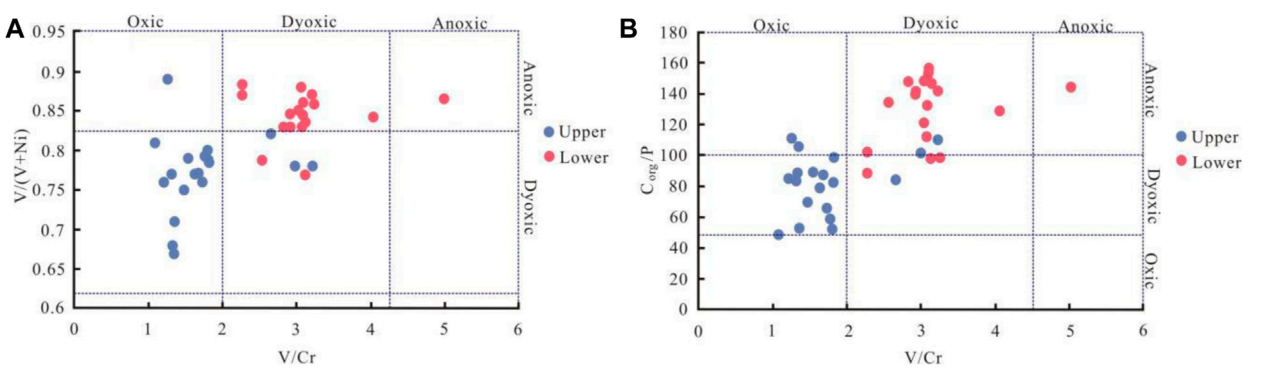

FIGURE 7
Crossplots diagram of the oxidation-reduction alternates of the Qing1 Member: **(A)** V/Cr ratios vs. V/(V+Ni) ratios, with cutoff values of 2–4.25 for V/Cr and 0.64–0.84 for V/(V+Ni) as divisions for paleoredox proxies; **(B)** V/Cr ratios vs. Corg/P ratios, with cutoff values of 2–4.25 for V/Cr and 50–100 for Corg/P as divisions for paleoredox proxies.

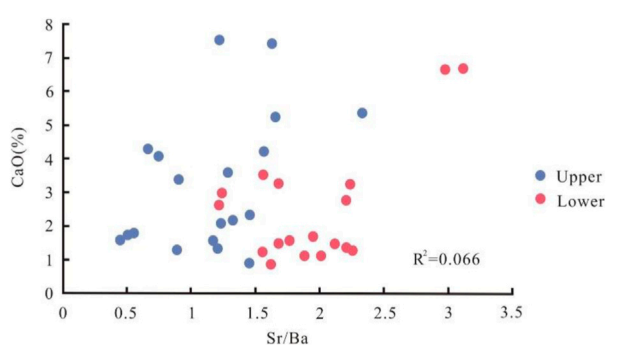

FIGURE 8
A poorly positive relevance between CaO and Sr/Ba.

makes it an important indicator in the study of paleoclimate (Yin et al., 2017; Zhao et al., 2016). When the climate is dry and the lake water is concentrated, it will enter the sediment first. Previous studies suggested that the Sr/Cu ratio is a sensible index for paleoclimate change (Yin et al., 2017). A Sr/Cu ratio of less than 5 indicates a warm and humid climate, while more than 10 indicates a dry and hot climate (Yin et al., 2017). It is 3.15–11.43 (average: 7.43) in the Qing1 Member, and the average values of the lower and upper parts are 5.4 and 9.2, respectively. As depicted in Figure 5A, increases from the bottom to the top indicate evolutions of paleoclimate from warm and humid to dry and hot in sediments of the Qing1 Member.

CIA is capable of being adopted as an alternative for the intensity of physical source chemical weathering (Nesbitt and Young, 1982). High CIA values represent a warm and humid climate and not *vice versa* (Yan et al., 2010; Liu et al., 2019). The mean CIA value (Table 3) in the lower part of the Qing1 member was 78.16–89.63 (average:84.52), which was considerably higher than that in the upper part (70.12–88.21, average:78.13). These values indicate that during the deposition of the lower Qing 1 member, the paleoclimate was warm and humid, leading to a high intensity of regional terrestrial chemical weathering (Figure 5B).

5.2.1 Terrigenous influx

Generally, when the inflow of terrigenous materials is relatively strong, the organic matter will be diluted, leading to a reduction in the concentration (Jin et al., 2020). On the contrary, the inflow of terrigenous materials can also bring additional nutrients into a lake's aquatic body, and the accompanying input of fine-grained materials can grasp organic matter into the sediment, thereby also promoting the enrichment of organic matter (Dittmar and Kattner, 2003; Lu et al., 2019). Hence, terrigenous inflow imposes a vital impact on organic matter enrichment.

Al, Ti, and Zr are mainly of clay mineral origin, are poorly mobile during weathering diagenesis, and are often used as important indicators of clastic influx (Tribovillard et al., 2006; Zhao et al., 2016). The Ti/Al ratio is considered a valid index of non-aluminosilicate influx, which is applied to identify the inflow of coarse fractions in sediments. The high Ti/Al ratio indicates that the more input of coarse grains, the higher the sedimentary rate (Li et al., 2017). Nevertheless, in certain environments, Al may be exhausted

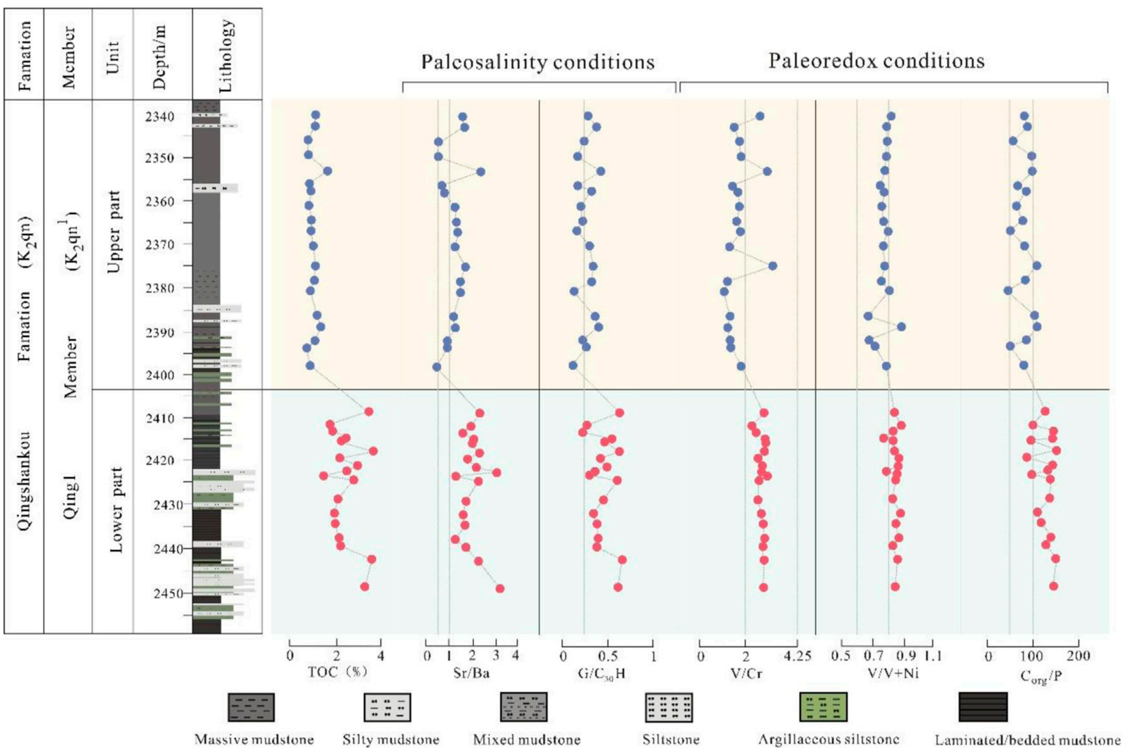

FIGURE 9
Variation curves of the paleosalinity conditions and paleoredox conditions alternate of the Qing1 Member.

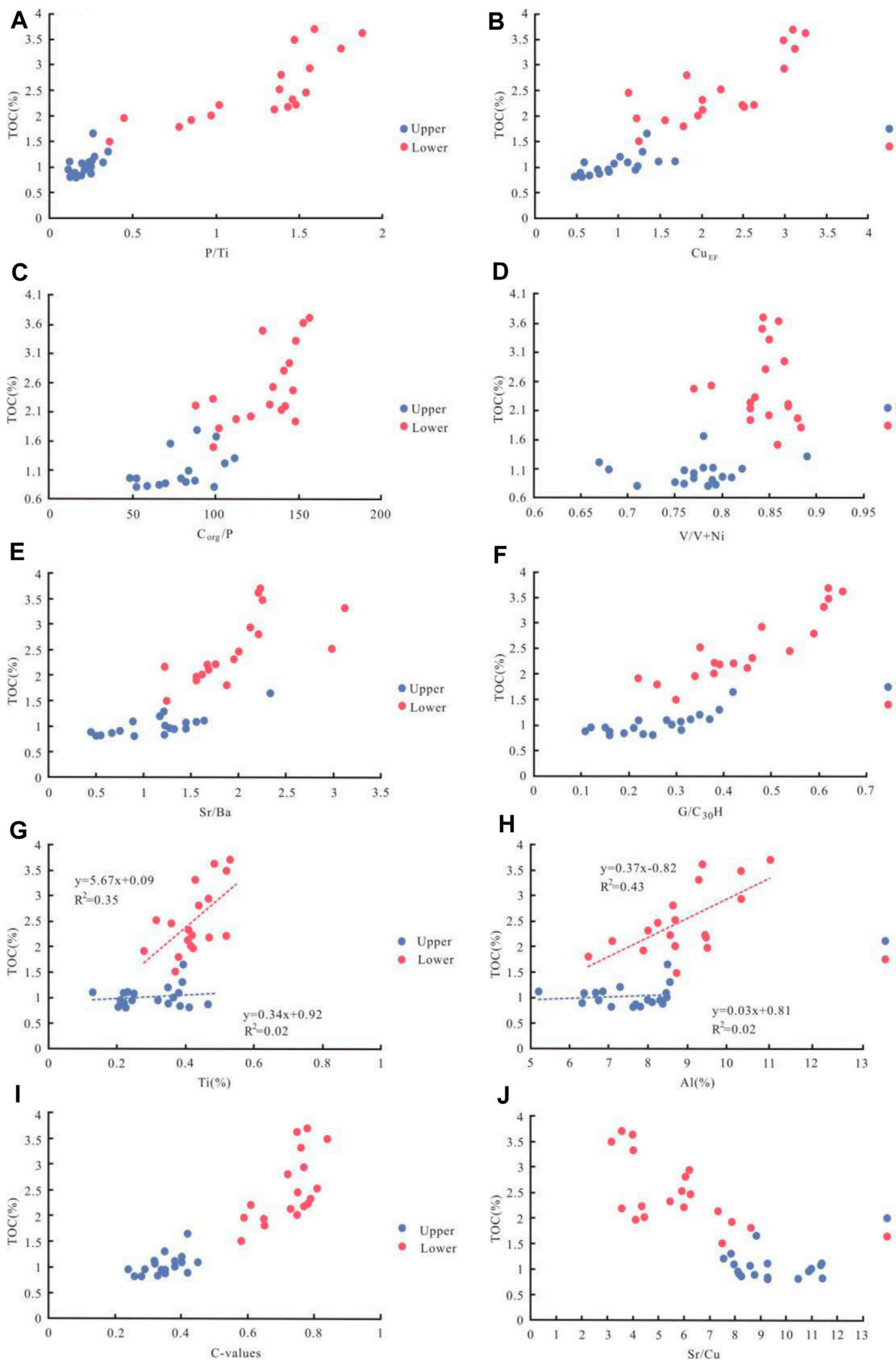

FIGURE 10
Crossplots of P/Ti ratios **(A)**, Cu_{ef} **(B)**, Corg/P **(C)**, V/V + Ni ratios **(D)**, Sr/Ba ratios **(E)**, $G/C_{30}H$ ratios **(F)**, Ti content **(G)**, Al content **(H)**, C values **(I)**, and Sr/Cu ratios **(J)** vs. TOC content.

or concentrated. Therefore, the method used to determine the terrestrial siliciclastic source of Al is to map the relationship between Al and Ti, Th, or Sc, and these elements are mainly derived from continental clasts. The good positive correlation observed in the Al–Ti cross plot (Figure 6) shows that most of the Al and Ti in the Qing1 Member part samples are derived from clastic rocks. Therefore, this element can be considered a useful assistant indicator to determine the inflow of terrestrial detritus rocks.

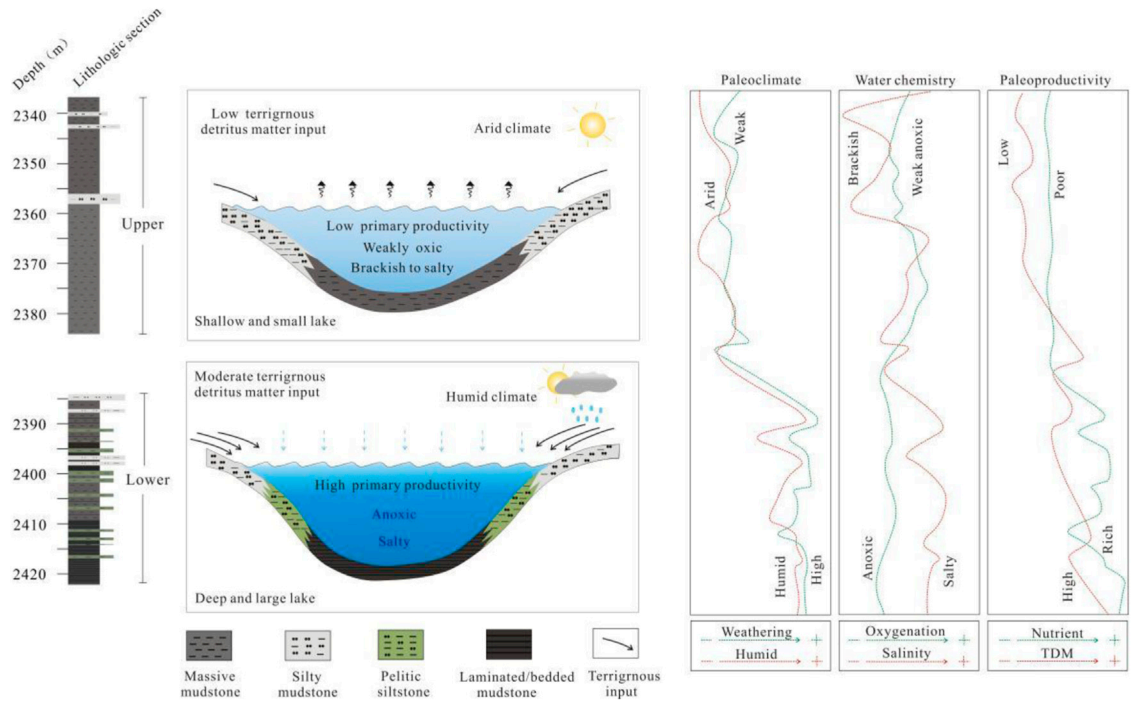

FIGURE 11
Sedimentary model demonstrating paleoredox, paleoproductivity, terrigenous influx, paleosalinity, paleoclimate, and the enrichment of OM in the shale of the Qing1 Member in the Changling Sag.

The concentration curves of Al and Ti in the Qing1 Member of the Changling Sag reflect the moderate and various terrigenous inputs (Figure 4). From the upper part to the lower part, the proportion mean values of Ti are 0.30% and 0.42%, respectively, and the proportion mean values of Al are 7.49% and 8.89%, respectively, showing a gradually increasing trend. The terrigenous input in the upper part is weak and relatively stable, and the terrigenous input in the lower part continues to increase, especially the coarse-grained material source. By analyzing the correlation between terrestrial inflow index and TOC content, it was concluded that there is no apparent relevance among the proportions of TOC, Al, and Ti in the upper part (Figure 10). It shows that the terrigenous inflow had no distinct influence on the accumulation of organic matter in this period. In the lower part, the correlation between TOC and terrigenous input (Al_2O_3) is obvious (R^2=0.43). The terrigenous input brings nutrients to the water body of the lake basin, which makes algae flourish, promotes paleoproductivity in the lake basin, and positively affects the organic matter enrichment.

5.3 Depositional environment

5.3.1 Paleoredox conditions

Differentiating paleoredox conditions is a major goal for paleoenvironmental research as these conditions have an important impact on the accumulation of organic matter and the emplacement of origin rocks (Algeo and Liu, 2020). The iron-group elements vanadium (V), nickel (Ni), and chromium (Cr) often present different valence states under different redox conditions. V exists 5 as pentavalent vanadate anions (HVO_4^{2-} or $H_2VO_4^{2-}$) in an oxidizing environment and can easily combine with the sediment to form precipitates. Conversely, Ni is easily adsorbed and enriched under reducing conditions, resulting in precipitation. Elemental Cr exists as hexavalent chromate anions (CrO_4^{2-}) in oxidizing environments and trivalent Cr^{3+}in reducing environments; thus, the element can easily combine with humic or fulvic acid to form complex compounds (Hatch and Leventhal, 1992; Pang et al., 2019). V/(V + Ni) and V/Cr are frequently utilized in identifying paleo oxygen facies in lake water. Therefore, the V/(V + Ni) and V/Cr ratios are commonly adopted to determine the redox conditions of the sedimentary environment. In detail, a high ratio of V/(V + Ni) (i.e., >0.84) suggests a strong stratified anoxic aquatic environment, a medium V/(V + Ni) value (0.54–0.82) suggests a low stratified anoxic bottom water condition, and a low ratio of V/(V+Ni) (i.e., 0.46–0.60) represents poorly stratified anoxic water body (Hatch and Leventhal, 1992). Hence, an increase in the V/(V+Ni) ratio may be indicative of increased hypoxia. A V/Cr ratio of <2, 2–4.25, and >4.25 respectively denote an oxic environment, a dysoxic environment, and an anoxic environment (Rimmer, 2004; Zhou et al., 2018). The V/(V + Ni) values of the upper Qing1 Member were recorded between 0.67 and 0.89 (average: 0.77), indicating a weakly reducing environment. Conversely, the V/(V+Ni) values of the lower Qing1 Member ranged from 0.77 to 0.88 (average: 0.84), indicating a weakly stratified reducing environment. V/Cr values of the upper Qing1 Member ranged from 1.09 to 3.21 (average: 1.73), indicating a weakly oxidizing environment. In contrast, the V/Cr values of the lower

Qing1 Member varied from 2.27 to 4.99 (mean 3.10), demonstrating a dysoxic environment. The cross plots of oxidation-reduction alternates display that the lower shale samples are primarily distributed in the dysoxic and partially anoxic zones, while the upper samples are primarily distributed in the weakly oxidizing and anoxic fields. The results also suggest that the lower part was generated under a comparatively anoxic/dysoxic environment, whereas the upper part was generated in weaker oxidizing conditions. In addition, the distribution characteristics of pristane and phytane can reflect the redox conditions of ancient lakes (Hu et al., 2010). The upper part of Pr/Ph is 0.57–0.9 (average for 0.74), and the lower part is 0.88–1.21 (average for 1.02), also indicating the weakly oxidizing environment and dysoxic environment, respectively.

Generally, by adsorption and complexation reactions and microbial storage of polyphosphates in sediments acting as authigenic phosphorus minerals, most of the phosphorus (P) produced by organic matter degradation is removed in an oxygenated water environment (Tian et al., 2019). At the same time, organic carbon (Corg) is largely degraded by microorganisms. In contrast, in the anoxic aqueous bodies, a mass of P related to Fe hydroxide is dispersed out of the sediment via reduction dissolution, which favors the preservation of organic carbon but not phosphorus (Algeo and Ingall, 2007). Therefore, the mole ratio of Corg/P in sediments formed in an anoxic environment is higher than that in an anoxic environment (Algeo and Liu, 2020). In this study, the Corg/P ratios of the Qing1 Member were between 48.71 and 156.48 (average:105.18), with a range of values from 88.15 to 156.48 for the lower section. Meanwhile, a range of variation from 48.71 to 111.23 was observed in the upper section. The ratio shows a gradual decrease from lower to upper, revealing that the lower shale was primarily sedimented in an anoxic to a dysoxic environment, while the upper shale generated predominantly in a dysoxic to a weak oxic environment (Figure 7).

5.3.2 Paleosalinity conditions

The chemical composition of the aquatic environments in lakes directly determines the oxidation-reduction conditions in the aquatic environment, including salinity and pH values (Tian et al., 2019). Palaeosalinity is an essential index for the reconstruction of the paleoenvironment in the process of origin rock deposition. During deposition, Sr is easier to move than Ba. In freshwater, Ba^{2+} is bound with SO_4^{2-} in brine to form $BaSO_4$ precipitation when freshwater and saltwater are intermixed. $SrSO_4$ is highly soluble, migrates further, and is biologically precipitated. Therefore, the ratio of Sr/Ba switches to a larger value with an increase in the distance from the coast (Wang et al., 2020). However, it should be clarified that when Sr/Ba is considered as the representative of paleosalinity, carbonate Sr does not change the signal (Wei and Algeo, 2020). Therefore, samples containing more than 4% CaO are ruled out. This can be attributed to the fact that Sr tends to replace Ca^{2+} in the $CaCO_3$ lattice (Liu et al., 2020; Wei and Algeo, 2020). Afterward, the residual samples were determined according to the cross plot of $CaCO_3$ and Sr/Ba. This showed a poor positive relevance (R^2=0.066) (Figure 8), which proves the effectiveness of Sr/Ba as an indicator of paleosalinity. In the present study, the values of all samples (ruling out samples with CaO content higher than 4%) exceeded 0.5, suggesting that all members were deposited in saline water (Liu et al., 2020). The Sr/Ba values in the upper Qing1 Member were between 0.45 and 2.33 (with an average of 1.16), which reveals the presence of saline water bodies. In contrast, the Sr/Ba values of the lower Qing1 Member were between 2.25 and 3.12 (with an average of 1.95). In the lower Qing1 Member, the paleosalinity was significantly greater than that in the upper part (Figure 9).

As the stratification of water bodies is mostly related to high salinity, the relative abundance of gammacerane indicates the salinity and stratification characteristics of sedimentary water bodies (Zhou et al., 2018). The gammacerane index ($Ga/C_{30}H$) of the lower part of the Qing1 Member varied in a range of 0.22 and 0.65 (with an average of 0.45) and that of the upper part ranged between 0.11 and 0.42 (with an average of 0.25). Thus, the paleosalinity of the latter is lower than that of the former, which is in line with the rule of trace elements. The paleosalinity index Sr/Ba was highly positively correlated with TOC contents (Figure 10). These results demonstrate that a salinized water environment is favorable for the release of organic matter and organic matter enrichment. Furthermore, preservation is well achieved in highly saline water.

5.3.3 Mechanisms of organic matter accumulation in the Qing1 Member

The enrichment of organic matter in lake sediments primarily relies on paleoclimate, paleoredox conditions, productivity, and detrital input. As the largest continental oil and gas basin in China, the Songliao Basin was greatly influenced by large-scale lake invasion and anoxic events in the Qing1 Member in the late Cretaceous (Feng et al., 2010), which greatly promoted the abundance of organisms. During the Qing1 Member of the Changling Sag, the lake basin entered the rapid settlement stage. The lake area suddenly expanded because of lake invasion, the lake level rose, and a deep water sedimentary environment developed.

The TOC content was positively related to both the value of V/V+Ni and the value of V/Cr (Figure 10), proving that organic matter accumulation in deposition is primarily regulated by benthic oxidation-reduction conditions. Reducing the bottom water conditions is more conducive to the conservation and enrichment of organic matter, while the condition of oxidized bottom water leads to easy consumption of organic matter and low TOC in the shale. The shales in the upper part seem to have been weakly sedimented in dysoxic to oxic conditions. On the contrary, the sediment in the lower part was deposited under anoxic and reductive conditions, which was favorable for the preservation of organic matter.

The positive correlation between TOC and P/Ti shows that the main generation is also a vital element in controlling the accumulation of organic matter of the Qing1 Member. A large amount of terrigenous organic matter may have been brought into the lake when the river system was established under comparatively warm or wet conditions, especially in the lower sedimentary period. Terrigenous influx provides a place for OM adsorption, so it is very beneficial to the preservation and concentration of OM.

The paleoclimate was relatively hot and dry in the depositional stage of the upper part of the Qing1 Member, which was not conducive to the development of peripheral vegetation and organisms in the basin. The paleoproductivity was at a relatively low level (P/Ti average 0.21), and the impact of terrigenous input was relatively small (R^2 value of TOC and Ti is 0.02) even though there were high reductive preservation conditions under the high salinity saline water body, due to its low paleoproductivity. Upper part is still unable to form high organic matter enrichment intervals (Figure 11). The lake of the Changling Depression deposited in the lower section of the Qing1 Member has the characteristics of a small water area, multiple sources, and near sources. The paleoclimate affects the water quality and source supply of the lake by changing the amount of sunlight and humidity. During this period, the paleoclimate was warm and humid. This was beneficial to the reproduction of organisms in the basin, improved the main generation of the lake basin, and promoted the reproduction and growth of surrounding vegetation. With the enhancement of chemical weathering, the input of terrigenous organic matter increased. At the time, the origin of organic matter was mixed source input. In terms of water preservation conditions, the salinity of the lake water medium is high, belonging to a brackish water saline environment. Thus it is easy to form salinity stratification and it is beneficial to the saving of organic matter. The organic matter enrichment mode belongs to the paleoproductivity preservation interaction mode under the joint action of high organic matter input and anoxic environment (Figure 11).

6 Conclusion

(1) The first member of the Qingshankou Formation in the Changling Sag, southern Songliao basin, was studied to gain an understanding of paleo-depositional environment controls on organic matter accumulation. Based on the TOC proportion, the shale in this exploration field can be classified into two parts, namely, with high TOC content in the lower section and low TOC proportion in the upper section.
(2) It is precisely due to changes in the sedimentary environment that there is a difference in the degree of organic matter enrichment between the upper and lower parts of the Qing1 Member. The lower part was under warm and humid climatic conditions, which were generated in the anoxic environment. Terrigenous input brought nutrients to the water body of the lake, made algae flourish, and led to a relatively high paleoproductivity of the lake. In contrast, the terrigenous inflow was relatively low in the upper part, which was mainly deposited under weak oxidizing conditions, with gradually enhanced oxidation and reduced productivity.
(3) In the upper part, under the relatively hot and dry paleoclimatic conditions, the paleoproductivity was low. Even if the preservation conditions were good, the enrichment degree of organic matter was still non-ideal. In the lower part, the warm and humid paleoclimate in this stage enhanced the primary productivity of the lake basin and improved the import of terrigenous organic matter. Additionally, the salinity of the lake water medium was high, which made it easy to form salinity stratification. Thus, this is beneficial to the preservation of organic matter.

Data availability statement

The original contributions presented in the study are included in the article/Supplementary Material, further inquiries can be directed to the corresponding author.

Author contributions

YM: paper writing, summary, and graphic drawing FJ: conducting experiments and processing experimental data. All authors contributed to the article and approved the submitted version.

Conflict of interest

The authors declare that the research was conducted in the absence of any commercial or financial relationships that could be construed as a potential conflict of interest.

Publisher's note

All claims expressed in this article are solely those of the authors and do not necessarily represent those of their affiliated organizations, or those of the publisher, the editors and the reviewers. Any product that may be evaluated in this article, or claim that may be made by its manufacturer, is not guaranteed or endorsed by the publisher.

References

Algeo, T. J., and Ingall, E. (2007). Sedimentary Corg:P ratios, paleocean ventilation, and Phanerozoic atmospheric pO_2. *Palaeogeogr. Palaeoclimatol. Palaeoecol.* 256 (3–4), 130–155. doi:10.1016/j.palaeo.2007.02.029

Algeo, T. J., and Li, C. (2020). Redox classification and calibration of redox thresholds in sedimentary systems. *Geochem. Cosmochim. Acta.* 287, 8–26. doi:10.1016/j.gca.2020.01.055

Algeo, T. J., and Liu, J. S. (2020). A re-assessment of elemental proxies for paleoredox analysis. *Chem. Geol.* 540, 119549. doi:10.1016/j.chemgeo.2020.119549

Algeo, T. J., and Maynard, J. B. (2004). Trace-element behavior and redox facies in core shales of Upper Pennsylvanian Kansas-type cyclothems. *Chem. Geol.* 206 (3–4), 289–318. doi:10.1016/j.chemgeo.2003.12.009

Carrol, A. R., and Bohacs, K. M. (1999). Stratigraphic classification of ancient lakes: balancing tectonic and climatic controls. *Geology* 27, 99–102. doi:10.1130/0091-7613(1999)027<0099:scoalb>2.3.co;2

Chen, C., Wang, J. S., Wang, Z., Peng, Y. B., Chen, X. H., Ma, X. C., et al. (2020). Variation of chemical index of alteration (CIA) in the Ediacaran Doushantuo Formation and its environmental implications. *Precambr. Res.* 347, 105829–105910. doi:10.1016/j.precamres.2020.105829

Dittmar, T., and Kattner, G. (2003). The biogeochemistry of the river and shelf ecosystem of the arctic ocean: A review. *Mar. Chem.* 83 (3–4), 103–120. doi:10.1016/s0304-4203(03)00105-1

Dong, T., He, S., Yin, S., Wang, D., Hou, Y., and Guo, J. (2015). Geochemical characterization of source rocks and crude oils in the upper cretaceous Qingshankou Formation, changling sag, southern Songliao Basin. *Mar. Petroleum Geol.* 64, 173–188. doi:10.1016/j.marpetgeo.2015.03.001

Feng, Z. Q., Jia, C. Z., Xie, X. N., Zhang, S., Feng, Z. H., and Timothy, A. (2010). Tectonostratigraphic units and stratigraphic sequences of the nonmarine Songliao Basin, northeast China. *Basin Res. (in Chin.* 22, 79–95. doi:10.1111/j.1365-2117.2009.00445.x

Harris, N. B., McMillan, J. M., Knapp, L. J., and Mastalerz, M. (2018). Organic matter accumulation in the upper Devonian Duvernay formation, western Canada sedimentary basin, from sequence stratigraphic analysis and geochemical proxies. Sediment. Geol. 376, 185–203. doi:10.1016/j.sedgeo.2018.09.004

Hatch, J. R., and Leventhal, J. S. (1992). Relationship between inferred redox potential of the depositional environment and geochemistry of the Upper Pennsylvanian (Missourian) Stark Shale Member of the Dennis Limestone, Wabaunsee County, Kansas, U.S.A. *ChemicalGeology* 99 (1-3), 65–82. doi:10.1016/0009-2541(92)90031-y

Holfmann, P., Ricken, W., Schwark, L., and Leythaeuser, D. (2000). Carbon-sulfur-iron relationships and 13C of organic matter for late Albian sedimentary rocks from North Atlantic Ocean: paleoceanographic implications. *Palaeogeogr. Palaeoclim. Palaeoecol.* 163, 97–113.

Hu, G. Y., Luo, X., Li, Z. S., Zhang, Y., Yang, C., Li, J., et al. (2010). Geochemical characteristics and origin of light hydrocarbons in biogenic gas. *Sci. China Earth Sci.* 53, 832–843. doi:10.1007/s11430-010-3072-6

Huang, Y., Yang, G., Gu, J., Wang, P., Huang, Q., Feng, Z., et al. (2013). Marine incursion events in the Late Cretaceous Songliao Basin: constraints from sulfur geochemistry records. *Palaeogeogr. Palaeoclimatol. Palaeoecol.* 385, 152–161. doi:10.1016/j.palaeo.2013.03.017

Jin, C., Liao, Z., and Tang, Y. (2020). Sea-level changes control organic matter accumulation in the Longmaxi shales of southeastern Chongqing, China. *Mar. Petrol. Geol.* 119, 104478. doi:10.1016/j.marpetgeo.2020.104478

Katz, B. J. (2005). Controlling factors on source rock development-a review of productivity, preservation and sedimentation rate. *SEPM Spec.* 82, 7–16.

Li, Y., Zhang, T., Ellis, G. S., and Shao, D. (2017). Depositional environment and organic matter accumulation of upper Ordovician–lower Silurian marine shale in the upper Yangtze platform, south China. *Paleogeogr. Paleoclimatol. Paleoecol.* 466, 252–264. doi:10.1016/j.palaeo.2016.11.037

Liu, B., Wang, H., Fu, X., Bai, Y., Bai, L., Jia, M., et al. (2019). Lithofacies and depositional setting of a highly prospective lacustrine shale oil succession from the Upper Cretaceous Qingshankou Formation in the Gulong sag, northern Songliao Basin, northeast China. *AAPG Bull.* 103, 405–432. doi:10.1306/08031817416

Liu, J., Cao, J., Hu, G., Wang, Y., Yang, R., and Liao, Z. (2020). Water-level and redox fluctuations in a Sichuan Basin lacustrine system coincident with the Toarcian OAE. *Palaeogeogr. Palaeoclimatol. Palaeoecol.* 558, 109942. doi:10.1016/j.palaeo.2020.109942

Liu, Z. H., Zhuang, X. G., Teng, G. E., Xie, X. M., Yin, L. M., Bian, L. Z., et al. (2015). The lower Cambrian Niutitang Formation at Yangtiao (Guizhou, SW China): organic matter enrichment, source rock potential, and hydrothermal influences. *J. Petrol. Geol.* 38 (4), 411–432. doi:10.1111/jpg.12619

Liu, Z. J., Wang, D. P., Liu, L., Liu, W. Z., Wang, P. J., Du, X. D., et al. (1993). Sedimentary characteristics of the Cretaceous in the Songliao Basin. *Acta Geol. Sin.* 6, 167–180.

Lu, Y., Jiang, S., Lu, Y., Xu, S., Shu, Y., and Wang, Y. (2019). Productivity or preservation? The factors controlling the organic matter accumulation in the late Katian through Hirnantian Wufeng organic-rich shale, South China. *Mar. Petrol. Geol.* 109, 22–35. doi:10.1016/j.marpetgeo.2019.06.007

McLennan, S. M. (1993). Weathering and Global Denudation. *J. Geol.* 101, 295–303. doi:10.1086/648222

Mizutani, S., Shao, J. A., and Zhang, Q. L. (1989). The Nadanhada Terrane in relation to mesozoic tectonics on continental Margins of East Asia. *Acta Geol. Sin.* 3, 204–216.

Mort, H., Jacquat, O., Adatte, T., Steinmann, P., Follmi, ¨ K., Matera, V., et al. (2007). The Cenomanian/Turonian anoxic event at the Bonarelli Level in Italy and Spain: enhanced productivity and/or better preservation. *Cretac.* Res. 28 (4), 597–612. doi:10.1016/j.cretres.2006.09.003

Naimo, D., Adamo, P., Imperato, M., and Stanzione, D. (2005). Mineralogy and geochemistry of a marine sequence, Gulf of Salerno, Italy. *Quat. Int.* 140-141, 53–63. doi:10.1016/j.quaint.2005.05.004

Nesbitt, H. W., and Young, G. M. (1982). Early Proterozoic climates and plate motions inferred from major element chemistry of lutites. *Nature* 299 (5885), 715–717. doi:10.1038/299715a0

Pang, S. Y., Cao, Y. C., and Liang, C. (2019). Lithofacies characteristics and sedimentary environment of the upper es4-lower Es3 in Dongying depression, Bohai Bay Basin - Taking well Fanye 1 as an example. *Petroleum Nat. gas Geol.* 40 (04), 799–809.

Peters, K. E., Walters, C. C., and Moldowan, J. M. (2005). *The biomarker guide: Biomarkers and isotopes in the environment and human history*. Cambridge: UK Cambridge University Press.

Pinedo, G. P., West, A. J., Tovar, A. A., Duarte, C. M., Marañón, E., Cermeño, P., et al. (2015). Surface distribution of dissolved trace metals in the oligotrophic ocean and their influence on phytoplankton biomass and productivity. *Glob. Biogeochem* 29, 1763–1781.

Price, J. R., and Velbel, M. A. (2003). Chemical weathering indices applied to weathering profiles developed on heterogeneous felsic metamorphic parent rocks. *Chem. Geol.* 202, 397–416.

Rimmer, S. M. (2004). Geochemical paleoredox indicators in Devonian–Mississippian black shales, central Appalachian basin (USA). *Chem. Geol.* 206 (3–4), 373–391. doi:10.1016/j.chemgeo.2003.12.029

Schmitz, B., Charisi, S. D., Thompson, E. I., and Speijer, R. P. (1997). Barium, SiO_2(excess), and P2O5 as proxies of biological productivity in the Middle East during the Palaeocene and the latest Palaeocene benthic extinction event. *Terra. Nova.* 9, 95–99. doi:10.1111/j.1365-3121.1997.tb00011.x

Schoepfer, S. D., Shen, J., Wei, H., Tyson, R. V., Ingall, E., and Algeo, T. J. (2015). Total organic carbon, organic phosphorus, and biogenic barium fluxes as proxies for paleomarine productivity. *Earth Sci. Rev.* 149, 23–52. doi:10.1016/j.earscirev.2014.08.017

Steiner, M., Wallis, E., Erdtmann, B. D., Zhao, Y., and Yang, R. (2001). Submarine-hydrothermal exhalative ore layers in black shales from South China and associated fossils insights into a Lower Cambrian facies and bio-evolution. *Palaeogeogr. Palaeoclimatol. Palaeoecol.* 169, 165–191. doi:10.1016/s0031-0182(01)00208-5

Tao, S., Xu, Y. B., Tang, D. Z., Xu, H., Li, S., Chen, S. D., et al. (2017). Geochemistry of the Shitoumei oil shale in the Santanghu Basin, Northwest China: implications for paleoclimate conditions, weathering, provenance and tectonic setting. Int. J. Coal Geol. 184, 42–56. doi:10.1016/j.coal.2017.11.007

Taylor, S. R., and McLennan, S. M. (1985). *The continental crust: Its composition and evolution*. Oxford: Blackwell Scientific Publications.

Tian, W., Wang, C. S., Bai, Y. S., and Li, P. J. (2019). Geochemical characteristics and organic matter accumulation mechanism of shetianqiao formation shale of Upper Devonian in Lianyuan sag, central Hunan. *Geoscience* 44 (11), 3794–3811.

Tribovillard, N., Algeo, T. J., Lyons, T., and Riboulleau, A. (2006). Trace metals as paleoredox and paleoproductivity proxies: an update. *Chem. Geol.* 232 (1–2), 12–32. doi:10.1016/j.chemgeo.2006.02.012

Tribovillard, N. P., Caulet, J. P., Vergnaud-Grazzini, C., Moureau, N., and Tremblay, P. (1996). Lack of organic matter accumulation on the upwelling-influenced Somalia margin in a glacial-interglacial transition. *Mar. Geol.* 133 (3–4), 157–182. doi:10.1016/0025-3227(96)00034-5

Tu, J. Q., Chen, J. P., Zhang, D. J., Cheng, K. M., Chen, J. J., and Yang, Z. M. (2012). A petrographic classification of macerals in lacustrine carbonate source rocks and their organic petrological characteristics: a case study on Jiuxi basin, NW China. *Acta Petrol. Sin.* 28 (3), 917–926.

Tyson, R. V. (2005). *The"productivity versus preservation"controversy: Cause, flaws and resolution*. Claremore: SEPM Special Publication.

Volkman, J. K., Barrett, S. M., Blackburn, S. I., Mansour, M. P., Sikes, E. L., and Gelin, F. (1998). Microalgal biomarkers: a review of recent research developments. *Org. Geochem.* 29, 1163–1179. doi:10.1016/s0146-6380(98)00062-x

Wang, P., Du, Y. S., Yu, W. C., Algeo, T. J., Zhou, Q., Xu, Y., et al. (2020a). The chemical index of alteration (CIA) as a proxy for climate change during glacial–interglacial transitions in Earth history. *Earth–Science Rev.* 201, 103032. doi:10.1016/j.earscirev.2019.103032

Wang, P. J., Mattern, F., Didenko, A. N., Zhu, D. F., Singer, B., and Sun, X. M. (2016). Tectonics and cycle system of the Cretaceous Songliao Basin: an inverted active continental margin basin. *Earth Sci. Rev.* 159, 82–102. doi:10.1016/j.earscirev.2016.05.004

Wang, Y. X., Xu, S., Hao, F., Zhang, B. Q., Shu, Z. G., Gou, Q. Y., et al. (2020b). Multiscale petrographic heterogeneity and their implications for the nanoporous system of the Wufeng-Longmaxi shales in Jiaoshiba area, Southeast China: response to depositional-diagenetic process. *GSA Bull.* 132, 1704–1721. doi:10.1130/b35324.1

Wang, B. (2023). Study on the differences in oil and gas transport characteristics of fault sand combination in the upper source and outer source slope areas: taking the songliao and bohai bay basins as examples[J]. *World Geology* 42 (3), 536–544.

Wei, W., and Algeo, T. J. (2020). Elemental proxies for paleosalinity analysis of ancient shales and mudrocks. *Geochem. Cosmochim.* Acta. 287, 341–366. doi:10.1016/j.gca.2019.06.034

Yan, D. T., Chen, D. Z., Wang, Q. C., and Wang, J. G. (2010). Large-scale climatic fluctuations in the latest Ordovician on the Yangtze block, south China. *Geology* 38, 599–602. doi:10.1130/g30961.1

Yin, J., Yu, Y. X., Jiang, C. F., Liu, J., and Zhao, Q. P. (2017). Geochemical characteristics of shale elements in Zhangjiatan, Ordos Basin and their relationship with organic matter enrichment. *J. coal Sci.* 42 (06), 1544–1556.

Zhang, C. C., Muirhead, J. D., Wang, H., Chen, S., Liao, Y. T., Lu, Z. S., et al. (2018). Lacustrine fan delta deposition alongside intrabasinal structural highs in rift basins: an example from the Early Cretaceous Jiuquan Basin, Northwestern China. *Int. J. Earth Sci.* 107 (5), 1835–1858. doi:10.1007/s00531-017-1575-5

Zhang, Y. P., Song, W. M., Na, F. C., Bao, Q. Z., and Wang, Y. (2016). Characteristics of the tectonic framework of northeast Asian mesozoic active continental margin. Geol. Resour. 25 (5), 407–422.

Zhao, Z. Y., Li, H. G., Wang, X. G., and Miao, H. B. (2004). A study on the mechanism of reservoir formation in the middle and shallow layers of the southern songliao basin [J]. *Petroleum Exploration and Development* 6, 17–19.

Zhao, J. H., Jin, Z. J., Jin, Z. K., Geng, Y. K., Wen, X., and Yan, C. N. (2016). Applying sedimentary geochemical proxies for paleoenvironment interpretation of organicrich shale deposition in the Sichuan Basin, China. *Int. J. Coal Geol.* 163, 52–71. doi:10.1016/j.coal.2016.06.015

Zhong, Q., and Yang, W. (1978). About Songliao Basin characterization of structural development (in Chinese). *Petroleum Explor. Dev.* 5, 50–52.

Zhou, L., Wang, Z. X., Li, H. J., and Hu, J. (2018). Shale organic matter enrichment model of niubutang formation of Lower Cambrian in East Sichuan Wuling Mountain Area. *J. geomechanics* 24 (05), 617–626.